Journal of Metals, Materials and Minerals, 35(4), e2379, 2025

Impacts of calcination temperature on the crystallography, granulometry and impedance of $LiCoMnO_4$

Chee Wayne TAN[1], Zul Hilmi CHE DAUD[2,*], Zainab ASUS[2], Mohd Hasbullah IDRIS[1], Izhari Izmi MAZALI[2] and Mohd Kameil ABDUL HAMID[2]

[1] *Faculty of Mechanical Engineering, Universiti Teknologi Malaysia, 81310 Johor Bahru, Johor, Malaysia*
[2] *Automotive Development Centre, Faculty of Mechanical Engineering, Universiti Teknologi Malaysia, 81310 Johor Bahru, Johor, Malaysia*

***Corresponding author e-mail**: hilmi@mail.fkm.utm.my

Received date:
22 April 2025
Revised date:
15 July 2025
Accepted date:
18 September 2025

Keywords:
Calcination;
Crystallography;
Granulometry;
Impedance;
$LiCoMnO_4$

Abstract

Spinel structured lithium cobalt manganese oxide ($LiCoMnO_4$) which exhibit reduction potential surpassing 5.0 V (vs. Li^0 | Li^+) was identified to be one of the prospective cathode candidates for next generation lithium-ion electrochemical systems. This article highlights the significance of calcination temperature on the crystallography of the resultant electroceramic compound as well as the corresponding response on the granulometry and impedance of $LiCoMnO_4$. $LiCoMnO_4$ compounds synthesised via sol-gel reaction in the first instance were converted into xerogel and subsequently subjected to facile one-step calcination protocol. Crystallography of the post-calcinated compounds were characterised via powder x-ray diffraction (XRD) technique. Temperature ranging between 600°C to 700°C was identified to be the critical process window which enabled the formation of single phase $LiCoMnO_4$. Granulometry of the $LiCoMnO_4$ compound synthesised at 600°C and 700°C were characterised in term of morphology and particle size distribution. $LiCoMnO_4$ calcinated at 600°C attained smaller particle size distribution and renders in relatively lower charge transfer impedance as compared to the specimen subjected to calcination at 700°C with relatively larger particle size distribution.

1. Introduction

The pursuit of high performance rechargeable lithium-ion electrochemical systems with elevated operational voltage through increased redox potential between electrodes has spurred research interest in spinel structured $Li\Omega_xMn_2$-xO_4 cathode active compounds [1,2]. The term "Ω" denotes low valance-state metal cations such as manganese (Mn), cobalt (Co), nickel (Ni), chromium (Cr), aluminium (Al), magnesium (Mg), titanium (Ti), gallium (Ga), germanium (Ge), copper (Cu), zinc (Zn) and iron (Fe) [1,3-10].

Among them, lithium cobalt manganese oxide ($LiCoMnO_4$) which exhibits cubic space group $Fd\bar{3}m$ spinel crystal structure, where Li^+ ions are located at the 8a tetrahedral sites, while Co^{3+} and Mn^{4+} ions are randomly distributed in the 16d octahedral sites [11,12] was reported to display by far the highest reduction potential ranging between 5.1 V to 5.6 V (vs. Li^0 | Li^+) [1, 13-15], thereby enabling electrochemical systems constructed with the spinel structured cathode compound to outperform its predecessors as well as coequal counterparts in terms of voltage output when paired with similar anode system [1,11,16]. Besides, it was also divulged that $LiCoMnO_4$ cathode subjected to only approximately 0.7% of volumetric change during intercalation and deintercalation of Li^+ ions, suggesting the compound to display exceptional dimensional stability during operation and potentially emerge as a viable positive electrode candidate for electrochemical systems with low capacity fading [1,17].

The application of $LiCoMnO_4$ cathode at the present time is hindered by unresolved compatibility issue with commercial carbonate-based electrolytes which display relatively narrow oxidative stability window and susceptible to decomposition when paired with lithium metal as well as graphite anode and operated above 4.3 V [18-21]. Nonetheless, various researchers have demonstrated notable breakthrough on fluorine-rich electrolyte system as well as solid-state electrolyte with elevated oxidative stability which could unleash the full potential of $LiCoMnO_4$ upon commercialisation [22-26]. Moreover. $LiCoMnO_4$ cathode may also potentially be coupled with lithium titanate ($Li_4Ti_5O_{12}$) anode to harvest the benefits from both electrodes while offsetting their drawbacks by elevating discharge voltage and allowing fast charging which is attractive for the adoption in applications which requires high power and fast charging capability such as energy storage systems for portable power tools and delivery drones [11,27].

$LiCoMnO_4$ cathode compound have been fabricated at research laboratory since 1998 leveraging on various synthesis techniques ranging from solid-state reaction [28-30] to flux method [31], sol-gel [11,32], hydrothermal [33], solvothermal [34] as well as co-precipitation [35]. However, it was suggested that the synthesis of $LiCoMnO_4$ cathode at high temperature may cause oxygen loss from the spinel lattice, thereby induce reduction of Mn^{4+} ions to Mn^{3+} ions which promote the formation of Li_2MnO_3 [13,36]. Multiple research attempts to compensate oxygen loss experienced by $LiCoMnO_4$ synthesised in elevated temperature by performing calcination of the cathode

active compound in oxygen enriched atmosphere as well as pure oxygen condition to produce Mn^{3+} free $LiCoMnO_4$ unfortunately have not been proven to be effective [13,37]. It was proposed that wet-chemical synthesis techniques such as sol-gel method which require lower calcination temperature as well as partial substitution of oxygen atoms loss with fluorine atoms could also potentially inhibit the formation of Li_2MnO_3 [13,32].

Windmüller *et al.* in 2017 first reported the effectiveness of fluorine doping in supressing, although did not completely eliminate the formation of secondary phase compound particularly Li_2MnO_3 within the primary spinel structured $LiCoMnO_4$ cathode compound synthesised via two-step solid state reaction [13]. The effort observed 6% reduction on the formation of Li_2MnO_3, which translate to 18% improvement in term of reversible capacity as well as substantially lower rate of capacity fading just by introducing additional 10 mol% of fluorine in comparison with undoped $LiCoMnO_4$ cathode synthesised via similar process [13]. Nevertheless, both Windmüller *et al.* as well as Liu *et al.* in 2018 and 2021 respectively speculated that the approach of fluorination via addition of lithium fluoride (LiF) may however indirectly contribute to excess of lithium content which reduce stability of spinel phase at high temperature and promote the formation of inactive secondary phases [13,36].

Moreover, Liu *et al.* in 2021 empirically demonstrated that reduction on the amount of excess lithium from 10 mol% to 2 mol% while maintaining similar mole fraction of fluorine reduced the formation of monoclinic Li_2MnO_3 phase further by approximately 3% in comparison with the fluorine doped $LiCoMnO_4$ specimens synthesised by Windmüller *et al.* in 2017 [13]. Liu *et al.* attained total yield of 92.2% $LiCoMnO_4$ which displayed approximately 85% of theoretical discharge capacity with 123.6 $mAh{\cdot}g^{-1}$ attained at 1C discharge rate [36].

Lin *et al.* in 2022 on the other hand demonstrated alternative fluorine doping technique by introducing additional 1 wt% of ammonium fluoride (NH_4F) as in the course of co-precipitation process which in principle could be performed without altering the stoichiometric ratio of reactants to synthesise $LiCoMnO_4$ and effectively supressed the formation of Li_2MnO_3 at [0 0 1] [35]. Building on these insights, we attempted the synthesise $LiCoMnO_4$ cathode compound by substituting conventional lithium precursor with lithium fluoride (LiF) inspired by the findings published by Windmüller *et al.* [13,38,39] to enable fluorination yet maintain the stoichiometry ratio of the chemical system without introducing additional chemical compounds nor excess lithium via sol-gel approach [40,41] and elucidate the influence of calcination on the temperature on its crystallographic, granulometric and impedance characteristic of the resultant compound.

2. Experimental

2.1 Synthesis

0.01 mol of lithium fluoride (LiF, Alfa Aesar), 0.01 mol of cobalt acetate tetrahydrate ($Co(CH_3COO)_2{\cdot}4H_2O$, R&M Chemicals) and 0.01 mol of manganese acetate tetrahydrate ($Mn(CH_3COO)_2{\cdot}4H_2O$, R&M Chemicals) precursors were completely hydrolysed in de-ionised water to attain colloidal solution formulated with Li:Co:Mn at stoichiometric ratio of 1:1:1 in a beaker. Citric acid monohydrate ($C_6H_8O_7{\cdot}H_2O$, R&M Chemicals) which serves as chelating agent was added into the mixture at molar ratio of $N(C_6H_8O_7{\cdot}H_2O)/Ncations = 2$ without controlling the pH value and homogenised by mechanical stirring at 500 rpm with ∅ 8 mm × 40 mm pivoted polytetrafluoroethylene (PTFE) encased magnetic stirrer for approximately 1.5 h at 90°C until integrated gelation network forms.

Sol-gel formed was converted into xerogel via dehydration in a forced convection oven operated at 90°C for 12 h to remove residual moisture before storage. 10 mg of xerogel specimen was sampled and subjected to thermogravimetric analysis (TGA, Shimadzu DTG-60H) at heating rate of $10°C{\cdot}min^{-1}$ from 30°C up to 1000°C in air to estimate the optimal temperature for calcination. Dehydrated xerogel was transferred into 150 mL capacity alumina crucible with lid followed by one-step calcination process at internal crucible temperature of 400°C, 500°C, 600°C, 700°C, 800°C and 900°C respectively in muffle furnace with effective chamber volume of 200 mm × 300 mm × 120 mm.

Calcination was performed at heating rate of $10°C{\cdot}min^{-1}$ to target temperature and dwell for 12 h followed by natural cooling to room temperature without facilitated by additional oxygen supply nor air circulation. The post-calcinated compounds were subjected to 10 h of continuous pulverisation by overfall ball milling in a ∅100 mm × 100 mm cylindrical vessel with ∅10 mm zirconia milling media. Rotational speed of the milling vessel was fixed at 60 rpm, while mass ratio of milling media:cathode active material was set at 10:1.

2.2 Crystallography & morphology characterisation

Crystallographic analysis was performed on the pulverised compounds via powder X-ray diffraction (XRD, Rigaku Smartlab) with Cu-Kα radiation operated at 40 kV and 40 mA. X-ray diffraction pattern of the resultant compounds was collected at 2θ angle ranging between 10° to 100° at 0.01° step width and scanning rate of $1°{\cdot}min^{-1}$. Mass fraction of resultant phases present within the post-calcinated was identified via Rietveld Refinement method with PDXL software package coupled with ICDD PDF4 database.

Microstructure of the $LiCoMnO_4$ compounds was inspected via Scanning Electron Microscopy (SEM, JEOL JSM-IT210) operated under ×5000 magnification in Secondary Electron mode at 30 Pa, 15 kV and 40% probe current. Granulometry of the specimens was characterised via laser diffraction particle size analyser (PSA, Malvern Panalytical Mastersizer 3000) operated in dry dispersion mode adhering to ISO 13320 standard and tapped density measured in accordance to ASTM B527. The specific surface area of the specimens was analysed via Brunauer–Emmett–Teller (BET, Thermo Scientific Surfer) technique.

2.3 Electrochemical Impedance Spectroscopy

Cathode slurries were formulated at mass ratio of resultant compound: conductive agent:binder = 8:1:1. Polyvinylidene difluoride (PVDF, Solvay Solef® 5130) binder was pre-dissolved with N-methyl-2-pyrrolidone (NMP, R&M Chemicals) solvent at mass fraction of 5:95 to form binder solution before subsequently blended with carbon black (Timcal Super P) as well as the synthesised cathode active compound. The homogenised cathode slurries were coated onto aluminium current collector with film applicator operated at aperture gap 150 μm followed

by drying in vacuum oven for 12 h to remove residual solvent and moisture before calendered to improve interparticle contact as well as adhesion between cathode and current collector, resulting in final cathode thickness of 20 ± 2 µm and ~3.35 mg·cm^{-2} mass loading of cathode active material on current collector.

The calendered cathodes were mechanically punched into ∅ 15 mm diameter disc and assembled into CR2032 format half-cell in argon enriched glove box with commercial ∅ 16 mm × 0.2 mm lithium metal anode, 25 µm polypropylene (PP) separator and 60 µL of 1 M lithium hexafluorophosphate ($LiPF_6$) electrolyte in aprotic solvent made up of ethylene carbonate (EC):diethyl carbonate (DEC) at volume ratio of 1:1. The assembled half-cell was evaluated via electrochemical impedance spectroscopy (EIS, Methrom Autolab) at frequency ranging between 0.1 Hz to 10 kHz with perturbation amplitude of 10 mV.

3. Results and discussion

3.1 Thermogravimetric analysis

Thermogravimetric analysis conducted on the xerogel specimen implied that empirical experiment designed to identify optimal calcination temperature for the formation of $LiCoMnO_4$ shall encompass temperature ranging between 400°C to 900°C corresponding to the final plateau region of the thermogram as shown in Figure 1. It was observed from the differential thermal analysis curve that $LiCoMnO_4$ xerogel experienced multiple endothermic reactions upon heating before entering crystallisation phase which starts at 400°C vicinity [42].

Initial mass loss experienced by the samples upon heating prior to 100°C was associated to the departure of residual moisture retained within the xerogel specimens. Subsequent mass loss was predominantly contributed by three stages of thermal decomposition at which eliminate substantial amount of organic compounds from the xerogel specimens. Meanwhile, no observable peaks which indicate the occurrence of exothermic reaction can be detected from differential thermal analysis curve throughout the heating from 30°C to 1000°C.

Preliminary thermal decomposition performed prior to the identified onset temperature of 440°C may be perceived as superfluous since subsequent calcination process which will essentially need to be performed at comparatively higher temperature as rationalised from thermogravimetric analysis (TGA) result. Furthermore, it was hypothesised that dwelling the cathode compounds at the right temperature setpoint under prolonged duration as necessary could simultaneously eliminate the presence of organic impurities while promoting the crystal growth of spinel structured $LiCoMnO_4$ compound.

3.2 Crystallography

X-ray diffraction patterns for all of the resultant compounds synthesised from identical chemical formulation via sol-gel technique but subsequently subjected to different calcination temperatures ranging from 400°C to 900°C were depicted in Figure 2. At a glance, it was apparent that majority of the post-calcinated specimens displayed well-defined peaks, suggesting the formation of well-crystallised resultant compounds.

Prominent X-ray diffraction peaks were observed at 2θ angle of 19°, 37° and 45° proximity corresponding to the [1 1 1], [3 1 1] and [4 0 0] crystal plane in the cubic spinel structure. Meanwhile, minor X-ray diffraction peaks were also detected at 2θ angle of 39°, 49°, 60°, 66° as well as 69° corresponding to [2 2 0], [2 2 2], [3 3 1], [5 1 1] and [4 4 0] crystal plane in the cubic spinel structure.

Nonetheless, the synthesised compounds exhibit remarkably distinctive response especially in term of the magnitude of diffraction intensity when subjected to different calcination temperature. The relative X-ray diffraction intensity of the synthesised cathode compounds steadily increased with calcination temperature starting from 400°C until eventually culminated at 600°C to 700°C vicinity. It was observed that the relative X-ray diffraction intensity of the resultant compounds substantially declined when calcination temperature was further increased to 800°C and 900°C due to significant reduction in the mass fraction of $LiCoMnO_4$. It was surmised that the occurrence of irreversible deoxygenation mechanism may have occurred from 750°C onwards [36], followed by loss of lithium as calcination temperature

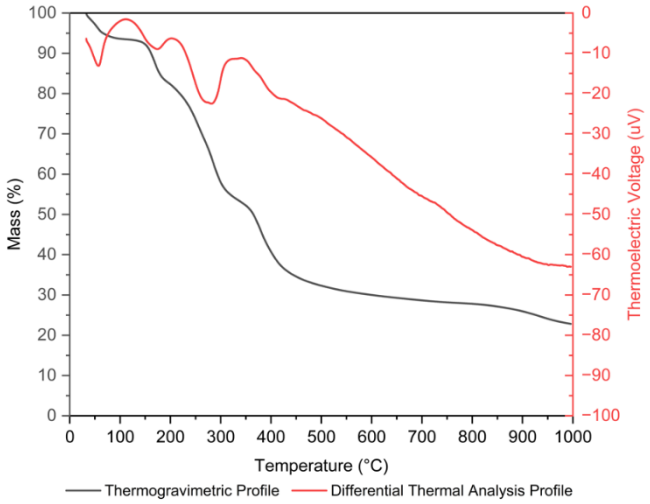

Figure 1. Thermogravimetric Analysis and Differential Thermal Analysis Profile.

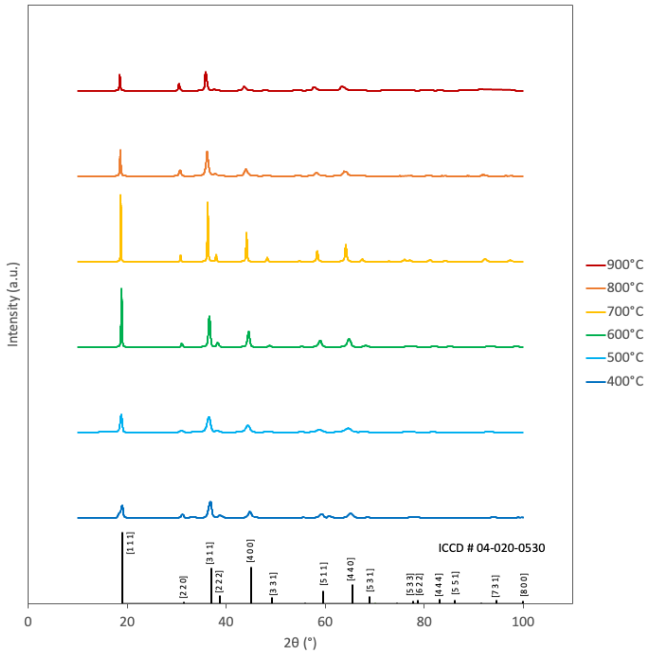

Figure 2. X-ray Diffraction Pattern.

were further elevated beyond 845°C [32] which resulted in the formation of secondary phase compounds and reduced the compositional presence of spinel structured $LiCoMnO_4$.

It may also be clearly distinguished from the close-up diffractogram in Figure 3 that the synthesised compounds experienced gradual drift in Bragg peaks position from higher to lower 2θ angle as calcination temperature were increased from 400°C to 900°C due to phase transformation and expansion of lattice structure resembling the findings reported by Windmüller *et al.* in 2018 [32]. The full width at half maximum (FWHM) corresponding to maximum peak intensity on the other hand reduced with the increment of calcination temperature from 400°C until 700°C as crystallinity improved, followed by the occurrence of peak broadening effect from 800°C onwards.

Table 1 evidently shown that $LiCoMnO_4$ compound calcinated at 600°C exhibit the highest I[111]/I[311] ratio that closely matched ICCD # 04-020-0530 with least deviation and expected to perform better than the specimen calcinated at 700°C especially operated at higher rate [43-45]. Meanwhile, the I[311]/I[400] ratio of $LiCoMnO_4$ compound calcinated at 600°C and 700°C are comparable with each other, but the index are comparatively greater [31,46], suggesting the compound might be prone to higher degree of tetragonal distortion [47,48].

Phase quantification via Rietveld refinement analysis as shown in Figure 4 revealed that the crystal growth of $LiCoMnO_4$ is primarily governed by calcination temperature which bear a resemblance to sigmoidal function. Calcination temperature of 400°C was experimentally proven to be insufficient for the formation of spinel structured $LiCoMnO_4$. Meanwhile, it was observed that $LiCoMnO_4$ start to form when subjected to calcination at 500°C but coexist with secondary phase $LiMn_2O_4$.

Only the presence of spinel structured $LiCoMnO_4$ was detected as $LiMn_2O_4$ diminished without the formation of other by-products when calcination was performed at 600°C. Similarly, only single-phase spinel structured $LiCoMnO_4$ was present within the resultant compound calcinated at 700°C. The composition of $LiCoMnO_4$ however rapidly subsided as the xerogel specimen was subjected to calcination at 800°C and 900°C.

It was experimentally validated that xerogel specimens need to be essentially subjected to at least 600°C in muffle furnace during calcination in order to effectively promote the formation of well-crystallised spinel structured $LiCoMnO_4$ with X-ray diffraction pattern that emulates diffractogram of single crystal $LiCoMnO_4$ synthesised by Hamada *et al.* [31]. Our findings also concurred with the observation reported by Amdouni *et al.* in 2006 despite different lithium precursor was adopted [42].

However, it was empirically deduced that the critical calcination temperature range which rendered the formation single-phase spinel structured $LiCoMnO_4$ via our synthesis approach is relatively narrow and shall ideally not exceed 700°C to prevent $LiCoMnO_4$ compound from entering declination phase. It is also crucial to note that albeit the $LiCoMnO_4$ specimens calcinated in both 600°C and 700°C are similar in term-of composition, they are not congruent as further discussed in section 3.3.

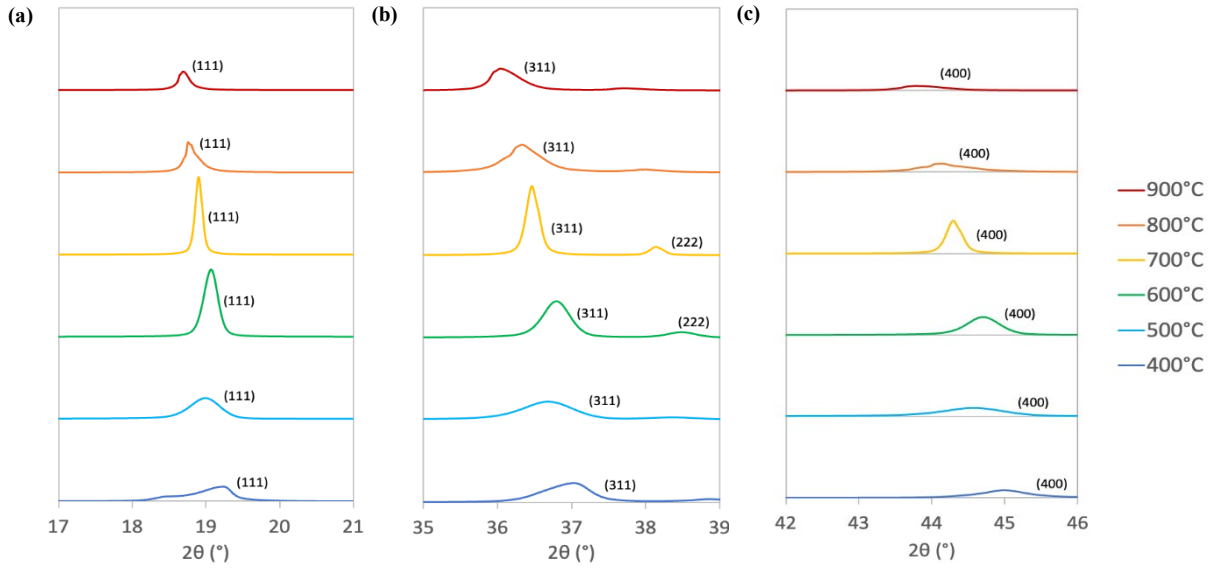

Figure 3. Diffractogram Focused at 2θ of (a) 17° to 21°, (b) 35° to 39°, and (c) 42° to 46°.

Table 1. Comparison of Peak Intensity and Relative Intensity Ratio.

Calcination Temperature [°C]	$I_{[111]}$	$I_{[311]}$	$I_{[400]}$	$I_{[111]}/I_{[311]}$	$I_{[311]}/I_{[400]}$
400	0.76	1.00	0.40	0.76	2.48
500	1.00	0.88	0.41	1.14	2.12
600	1.00	0.54	0.27	1.86	2.00
700	1.00	0.89	0.43	1.13	2.07
800	1.00	0.93	0.28	1.08	3.29
900	0.85	1.00	0.21	0.85	4.71
ICCD # 04-020-0530	1.00	0.49	0.50	2.03	0.98

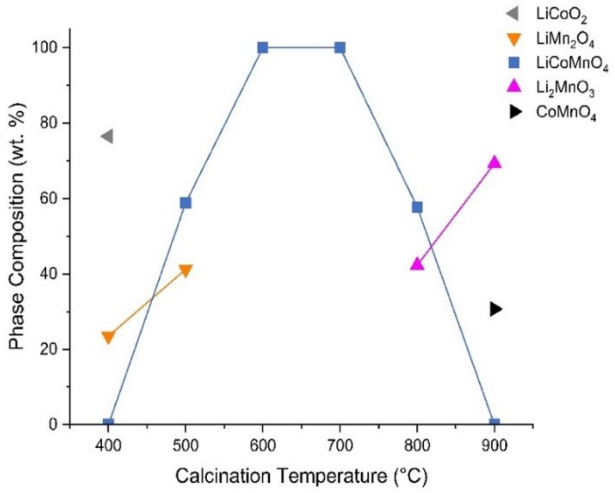

Figure 4. Phase Quantification via Rietveld Refinement.

Significant reduction in the composition of $LiCoMnO_4$ were observed from the specimens subjected to calcination at 800°C due to the tendency for the occurrence of deoxygenation mechanism [17] at higher temperature which promote formation of monoclinic phase Li_2MnO_3 as inferred by drastic decline of relatively diffraction intensity at [1 1 1] and pronounced shift in 2θ angle peak intensity position of [0 0 1] due to phase transformation [35]. Spinel phase $LiCoMnO_4$ completely diminished from the resultant compound calcinated at 900°C due to depletion of lithium from the spinel structured compound associated to the melting and fluxing effect of LiF which adhere to alumina crucible from 845°C onwards, resulting in the formation of lithium deficit rock-salt structured Co_2MnO_4 which co-exist with deoxygenated monoclinic phase Li_2MnO_3 in agreement with the findings reported previously by Windmüller *et al.* in 2018 [32].

3.3 Morphology and granulometry

Morphology evaluation performed via Scanning Electron Microscopy (SEM) as shown in Figure 5 qualitatively validated that specimens calcinated at both 600°C and 700°C attained single-phase compound with relatively homogenous grain size. However, it was observed that the specimen subjected to higher calcination temperature experienced greater crystal growth kinetics which resulted in comparatively larger grain size in agreement with experimental findings previously reported by various researchers on other spinel structured cathode compounds, particularly $LiMn_2O_4$ [49-51] and $LiNi_{0.5}Mn_{1.5}O_4$ [52, 3] as well as conventional layered structured $LiNi_xMn_yCo_zO_2$ cathode compound [54].

Quantitative granulometry analysis performed via laser scattering approach based on ISO 13320 standard as shown in Figure 6 inferred that the resultant compounds calcinated at both 600°C and 700°C displayed asymmetric particle size distribution trend despite both temperature setpoints resulted in the formation of single-phase $LiCoMnO_4$. The resultant compound calcinated at 600°C displayed two perceptible volume density peaks resembling bimodal particle size distribution trend due to higher surface energy of small particles which promote undesirable agglomeration [55]. Meanwhile, the volume weighted particle size distribution of the $LiCoMnO_4$ calcinated at 700°C was observed to be negatively skewed as compared to the specimen subjected to calcination at 600°C, resulting in less discernible secondary peak potentially due to inherently larger particle size distribution which are less susceptible to agglomeration.

The mode circular equivalent diameter value corresponding to the peak volume density of the resultant $LiCoMnO_4$ compound notably increased with calcination temperature, in agreement with the morphology evaluation performed via scanning electron microscopy. The existence of monotonic shoulder peak within both specimens may be potentially attributed by agglomeration effect of fine $LiCoMnO_4$ [56-58].

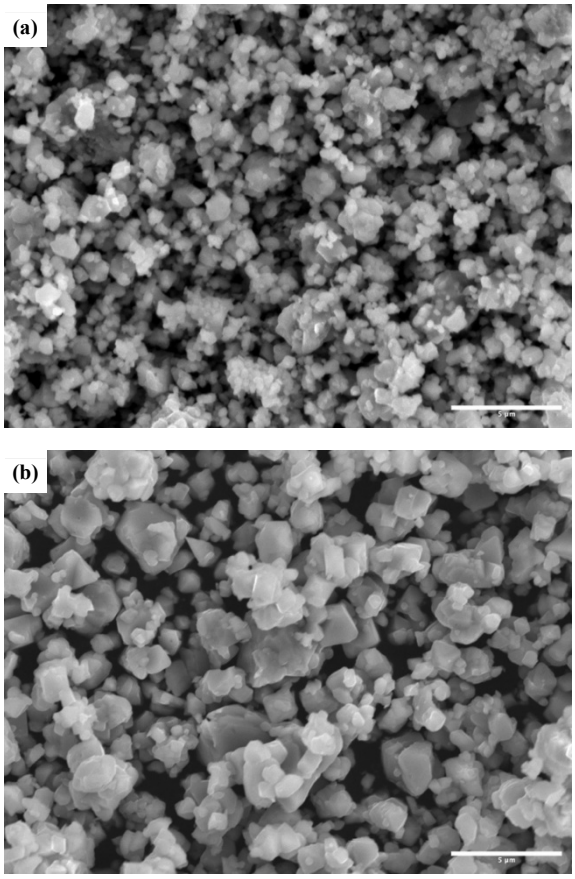

Figure 5. Microstructure of $LiCoMnO_4$ Calcinated at (a) 600°C, and (b) 700°C.

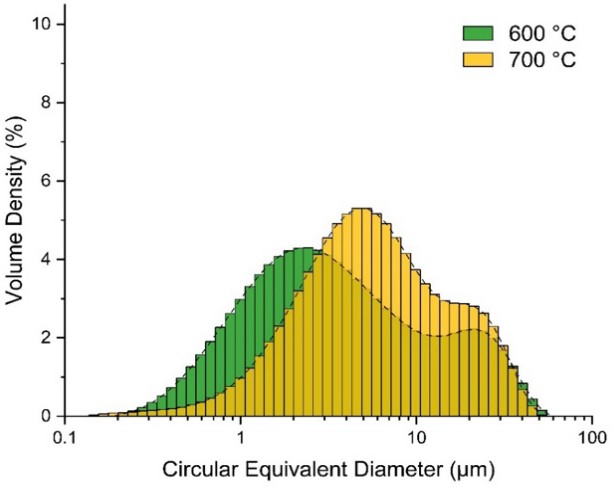

Figure 6. Particle Size Distribution of $LiCoMnO_4$.

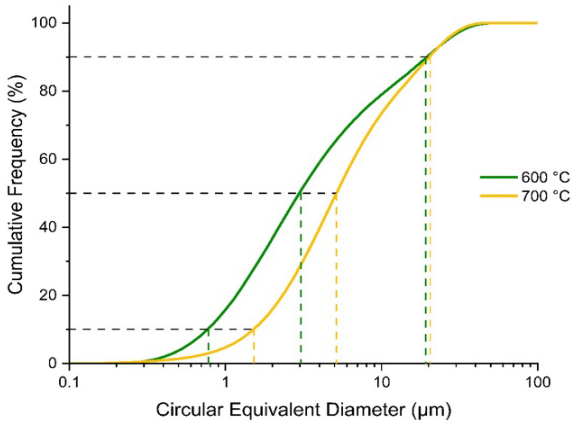

Figure 7. Cumulative Particle Size Distribution of $LiCoMnO_4$.

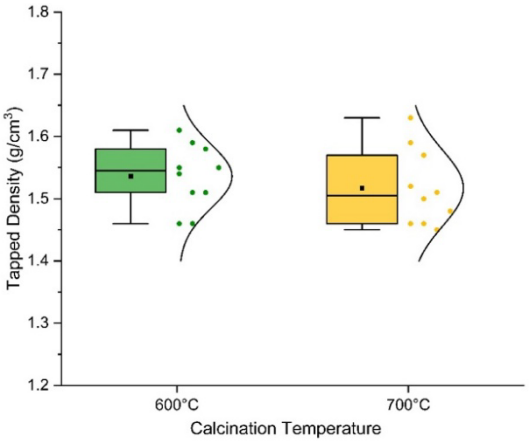

Figure 8. Tapped Density Distribution of $LiCoMnO_4$.

The 10th, 50th and 90th percentile circular equivalent diameter which are also commonly abbreviated as Dv10, Dv50 and Dv90 computed from the cumulative frequency distribution of the pulverised compounds as shown in Figure 7 were reported in Table 2 alongside with De Brouckere mean diameter or volume weighted moment mean diameter (Dvm). Other relevant parameters including particle size span, uniformity coefficient and specific surface area were also tabulated.

The mean and median tapped density of $LiCoMnO_4$ specimens synthesised via sol-gel approach from our experiment are relatively lower than value reported by Lin *et al.* in 2022 synthesised via co-precipitation technique [35]. Whilst the resultant compound calcinated at lower temperature appeared to attain higher tapped density with narrower distribution, t-test performed with p-value outcome of 0.56 suggested that the slight difference in tapped density population of $LiCoMnO_4$ specimens calcinated at both 600°C and 700°C are not statistically significant from one another.

Granulometry analysis performed on the post-calcinated compound indicated that we have not attained perfectly monodispersed particle size distribution which could be a contributing factor to downstream processing challenges observed, particularly in obtaining uniform slurry coating. $LiCoMnO_4$ cathode compound shall be adequately de-agglomerated to ensure uniform dispersion in binder during subsequent slurry batching process which enable higher particle packing fraction and mass loading of cathode active material on current collector [59-61]. It was proposed that the particle size distribution shall be further improved in the future with optimised pH level during sol-gel reaction, calcination temperature and regrinding procedure [35,55].

3.4 Electrochemical Impedance Spectroscopy

Electrochemical impedance spectroscopy (EIS) performed on the assembled half-cells at 0.1 Hz to 10 kHz revealed three frequency-dependent electrochemical processes. It was observed from the high frequency region in the Nyquist plot in Figure 9 that the intercept with the real axis which represents the bulk ohmic resistance are generally low in both specimens, but noticeably decreased from 3.92 Ω for the sample calcinated at 600°C to 1.84 Ω for the sample calcinated at 700°C despite the electrolyte and separator used [62] as well as assembly conditions are identical.

It was deduced that the higher bulk resistance observed for the $LiCoMnO_4$ cathode compound calcinated at 600°C from the fitted equivalent circuit diagram may be associated with presence of more grain boundaries as well as agglomeration of finer primary particles which hindered the penetration of electrolyte into electrode, thereby resulting in higher ohmic loss. Half-cells constructed with $LiCoMnO_4$ cathode compound subjected to calcination at both 600°C and 700°C respectively also displayed minute, but notable semicircular arc at middle frequency corresponding to electrical resistance contributed by the formation of solid electrolyte interface (SEI) layer [62].

Since both half-cells have not been subjected to galvanostatic cycling prior to electrochemical impedance spectroscopy analysis, resistance induced by the formation of SEI inferred potential occurrence of chemical reactions between cathode and electrolyte. Whilst SEI inevitably formed in both specimens upon exposure to electrolyte, $LiCoMnO_4$ cathode compound subjected to calcination at 600°C which possessed relatively higher specific surface area promoted the formation electrically insulative layer [63,64], resulting in higher interfacial resistance of 12.1 Ω and as compared to 8.84 Ω for the specimen calcinated at 700°C .

Table 2. Granulometry Information.

Calcination Temperature [°C]	600	700
Dv10 [μm]	0.77	1.45
Dv50 [μm]	3.12	5.21
Dv90 [μm]	18.70	21.20
Dvm [μm]	7.56	9.24
Span [μm]	5.75	4.31
Particle uniformity coefficient	1.737	1.041
Specific surface area [$m^2 \cdot g^{-1}$]	1.963	1.288
Tapped density [$g \cdot cm^{-3}$]	1.54 ± 0.05	1.52 ± 0.06

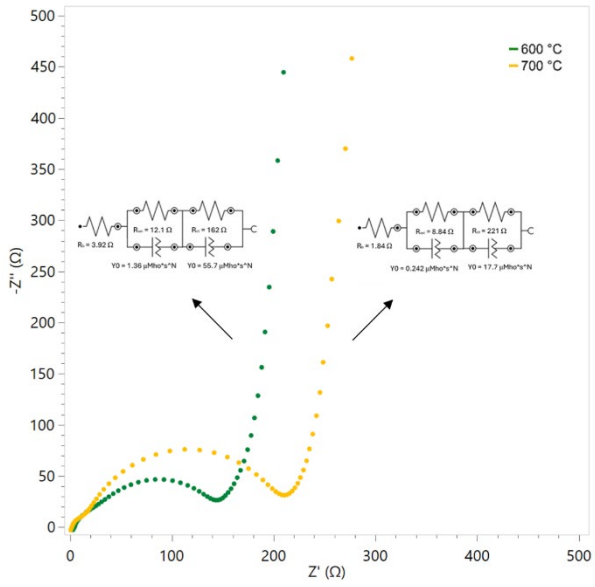

Figure 9. Nyquist Plot.

Meanwhile, the overall impedance of the electrochemical system is primarily governed by charge-transfer resistance at low frequency region. It was observed that $LiCoMnO_4$ cathode compound subjected to calcination at 600°C displayed relatively lower charge transfer resistance of 162 Ω as compared to 221 Ω for the sample calcinated at 700°C due to smaller particle size distribution and significantly higher specific surface area which facilitate Li^+ ion diffusion kinetics and potentially manifest in better electrochemical rate performance [58,65]. The Warburg impedance attributed by diffusion of lithium-ion within the host for both $LiCoMnO_4$ cathode compounds calcinated at 600°C and 700°C observed at the low frequency end appeared to be steep and comparable to each other [62,63].

Nonetheless, the charge transfer resistance shall be monitored as electrochemical systems constructed with smaller particle size as well as higher specific area could be subjugated by electrically resistive cathode-electrolyte interface which developed upon cycling [66,67]. Meanwhile, $LiCoMnO_4$ subjected to calcination at 700°C which exhibit comparatively larger particle size and lower specific surface area could be less susceptible to cationic dissolution distribution and contribute to better electrochemical cycling stability [58,65]. Manipulation of calcination temperature within the critical process window of 600°C to 700°C may also potentially be useful for granulometry control, particularly particle size distribution and specific surface area of single-phase $LiCoMnO_4$ for optimisation of electrochemical performance [54,68].

4. Conclusion and recommendation

It was demonstrated that single-phase spinel structured $LiCoMnO_4$ cathode active material can be successfully synthesised via sol-gel technique with the adoption of LiF as lithium precursor. It was inferred that calcination temperature exhibits direct corelation to the crystallography, granulometry and impedance of $LiCoMnO_4$. The critical temperature range which enabled the formation of single-phase $LiCoMnO_4$ cathode compound via one-step calcination protocol was pin-pointed to be 600°C to 700°C although agglomeration of particle is evidently inevitable with our existing protocol. We will explore the technical feasibility of further optimizing the granulometry of $LiCoMnO_4$ through pH control, calcination duration and pulverization parameters.

Acknowledgements

This research was funded by a grant from Research University Grant (UTM Matching Grant: Q.J130000.3024.04M84).

References

[1] N. Reeves-McLaren, M. Hong, H. Alqurashi, L. Xue, J. Sharp, A. J. Rennie, and R. Boston, "The spinel $LiCoMnO_4$: 5V cathode and conversion anode," *Energy Procedia*, vol. 151, pp. 158-162, 2018.

[2] R. Marom, S. F. Amalraj, N. Leifer, D. Jacob, and D. Aurbach, "A review of advanced and practical lithium battery materials," *Journal of Materials Chemistry*, vol. 21, no. 27, pp. 9938-9954, 2011.

[3] C. M. Julien, and A. Mauger, "Review of 5-V electrodes for Li-ion batteries: Status and trends," *Ionics*, vol. 19, no. 7, pp. 951-988, 2013.

[4] D. Liu, W. Zhu, J. Trottier, C. Gagnon, F. Barray, A. Guerfi, A. Mauger, H. Groult, C. M. Julien, J. B. Goodenough, and K. Zaghib, "Spinel materials for high-voltage cathodes in Li-ion batteries," *RSC Advances*, vol. 4, no. 1, pp. 154-167, 2014.

[5] H. F. Lin, S. T. Cheng, D. Z. Chen, N. Y. Wu, Z. X. Jiang, and C. T. Chang, "Stabilizing Li-rich layered cathode materials using a $LiCoMnO_4$ spinel nanolayer for Li-Ion batteries," *Nanomaterials*, vol. 12, no. 19, p. 3425, 2022

[6] K. Dai, J. Mao, Z. Li, Y. Zhai, Z. Wang, X. Song, V. Battaglia, and G. Liu, "Microsized single-crystal spinel LAMO for high-power lithium ion batteries synthesized via polyvinylpyrrolidone combustion method," *Journal of Power Sources*, vol. 248, pp. 22-27, 2014.

[7] T. Ohzuku, K. Ariyoshi, S. Takeda, and Y. Sakai, "Synthesis and characterization of 5 V insertion material of $Li[Fe_yMn_{2-y}]O_4$ for lithium-ion batteries," *Electrochimica Acta*, vol. 46, pp. 2327-2336, 2001.

[8] C. Sigala, A. Verbaere, J. L. Mansot, D. Guyomard, Y. Piffard, and M. Tournoux, "The Cr-substituted spinel Mn oxides $LiCr_yMn_{2-y}O_4$ ($0<y<1$): Rietveld analysis of the structure modifications induced by the electrochemical lithium deintercalation," *Journal of Solid State Chemistry*, vol. 132, pp. 372-381, 1997.

[9] J. Akimoto, Y. Gotoh, and Y. Takahashi, "Crystal growth of spinel-type $LiM_xMn_{2-x}O_4$ (M = Cr, Co, Ni) in High-temperature molten chlorides," *Crystal Growth & Design*, vol. 3, pp. 627-629, 2003.

[10] J. T. Son, and H. G. Kim, "New investigation of fluorine-substituted spinel $LiMn_2O_4$–F by using sol–gel process," *Journal of Power Sources*, vol. 147, no. 1-2, pp. 220-226, 2005.

[11] X. Huang, M. Lin, Q. Tong, X.,Li, Y.,Ruan, and Y. Yang, "Synthesis of $LiCoMnO_4$ via a sol–gel method and its application in high power $LiCoMnO_4/Li_4Ti_5O_{12}$ lithium-ion batteries," *Journal of Power Sources*, vol. 202, pp. 352-356, 2012.

[12] H. Chen, X. Yang, P.-S. Zhang, L. Liang, Y.-Z. Hong, Y.-J. Wei, G. Chen, F. Du, and C.-Z. Wang, "Observation of spin glass transition in spinel $LiCoMnO_4$," *Chinese Physics B*, vol. 24, no. 12, pp. 1275011-1275015, 2015.

[13] A. Windmüller, C.-L. Tsai, S. Möller, M. Balski, Y. J. Sohn, S. Uhlenbruck, and O. Guillon, "Enhancing the performance of high-voltage $LiCoMnO_4$ spinel electrodes by fluorination," *Journal of Power Sources*, vol. 341, pp. 122-129, 2017.

[14] Y. Arinicheva, M. Wolff, S. Lobe, C. Dellen, D. Fattakhova-Rohlfing, O. Guillon, D. Böhm, F. Zoller, R. Schmuch, J. Li, M. Winter, E. Adamczyk, and V. Pralong, "Ceramics for electrochemical storage," in *Advanced Ceramics for Energy Conversion and Storage*, pp. 549-709, 2020.

[15] C. Dräger, F. Sigel, S. Indris, D. Mikhailova, L. Pfaffmann, M. Knapp, and H. Ehrenberg, "Delithiation/relithiation process of $LiCoMnO_4$ spinel as 5 V electrode material," *Journal of Power Sources*, vol. 371, pp. 55-64, 2017.

[16] F. Schipper, E. M. Erickson, C. Erk, J.-Y. Shin, F. F. Chesneau, and D. Aurbach, "Review—recent advances and remaining challenges for lithium ion battery cathodes," *Journal of The Electrochemical Society*, vol. 164, no. 1, pp. A6220-A6228, 2016.

[17] K. Ariyoshi, H. Yamamoto, and Y. Yamada, "Synthesis optimization of electrochemically active $LiCoMnO_4$ for high-voltage lithium-ion batteries," *Energy & Fuels*, vol. 35, no. 16, pp. 13449-13456, 2021.

[18] Z. I. Radzi, V. Balakrishnan, A. K. Pandey, M. Z. Kufian, N. A. Rahim, S. R. S. Raihan, and S. Ramesh, "Structural, electrical and electrochemical characterization of hybrid morphological $LiNi_{0.5}Mn_{1.5}O_4$ cathode material," *Physica B: Condensed Matter*, vol. 624, pp. 1-14, 2022.

[19] K. Guo, S. Qi, H. Wang, J. Huang, M. Wu, Y. Yang, X. Li, Y. Ren, and J. Ma, "High-voltage electrolyte chemistry for lithium batteries," *Small Science*, vol. 2, no. 5, pp. 1-18, 2022.

[20] Z. Wang, J. Chen, J. Fu, Z. Li, and X. Guo, "Polymer-based electrolytes for high-voltage solid-state lithium batteries," *Energy Materials*, vol. 4, no. 4, pp. 1-24, 2024.

[21] L. Dong, S. Zhong, B. Yuan, Y. Ji, J. Liu, Y. Liu, C. Yang, J. Han, and W. He, "Electrolyte engineering for high-voltage lithium metal batteries," *Research*, vol. 2022, pp. 1-52, 2022.

[22] C. Zhang, "High-voltage electrolytes," *Nature Energy*, vol. 4, no. 5, pp. 350, 2019.

[23] L. Chen, X. Fan, E. Hu, X. Ji, J. Chen, S. Hou, T. Deng, J. Li, D. Su, X. Yang, and C. Wang, "Achieving high energy density through increasing the output voltage: A highly reversible 5.3 V battery," *Chem*, vol. 5, no. 4, pp. 896-912, 2019.

[24] L. Xia, Y. Xia, C. Wang, H. Hu, S. Lee, Q. Yu, H. Chen, and Z. Liu, "5 V-class electrolytes based on fluorinated solvents for Li-ion batteries with excellent cyclability," *ChemElectroChem*, vol. 2, no. 11, pp. 1707-1712, 2015.

[25] W.-H. Hou, Y. Lu, Y. Ou, P. Zhou, S. Yan, X. He, X. Geng, and K. Liu, "Recent advances in electrolytes for high-voltage cathodes of lithium-ion batteries," *Transactions of Tianjin University*, vol. 29, no. 2, pp. 120-135, 2023.

[26] X. Fan, X. Ji, L. Chen, J. Chen, T. Deng, F. Han, J. Yue, N. Piao, R. Wang, X. Zhou, X. Xiao, L. Chen, and C. Wang, "All-temperature batteries enabled by fluorinated electrolytes with non-polar solvents," *Nature Energy*, vol. 4, no. 10, pp. 882-890, 2019.

[27] H. Xia, Z. Luo, and J. Xie, "Nanostructured lithium titanate and lithium titanate/carbon nanocomposite as anode materials for advanced lithium-ion batteries," *Nanotechnology Reviews*, vol. 3, no. 2, pp. 161-175, 2014.

[28] K. Ariyoshi, H. Yamamoto, and Y. Yamada, "High dimensional stability of $LiCoMnO_4$ as positive electrodes operating at high voltage for lithium-ion batteries with a long cycle life," *Electrochimica Acta*, vol. 260, pp. 498-503, 2018.

[29] N. Reeves-McLaren, J. Sharp, H. Beltran-Mir, W. M. Rainforth, and A. R. West, "Spinel-rock salt transformation in $LiCoMnO_4$-δ," *Proceedings of the Royal Society A*, vol. 472, no. 2185, pp. 1-20, 2016.

[30] H. Kawai, M. Nagata, H. Tukamoto, and A. R. Westa, "A new lithium cathode $LiCoMnO_4$ toward practical 5 V lithium batteries," *Electrochemical and Solid-State Letters*, vol. 1, no. 5, 1999.

[31] Y. Hamada, N. Hamao, K. Kataoka, N. Ishida, Y. Idemoto, and J. Akimoto, "Single crystal synthesis, crystal structure and electrochemical property of spinel-type $LiCoMnO_4$ as 5V positive electrode materials," *Journal of the Ceramic Society of Japan*, vol. 124, no. 6, pp. 706-709, 2016.

[32] A. Windmüller, C. Dellen, S. Lobe, C.-L. Tsai, S. Möller, Y. J. Sohn, N. Wettengl, M. Finsterbusch, S. Uhlenbruck, and O. Guillon, "Thermal stability of 5 V $LiCoMnO_4$ spinels with LiF additive," *Solid State Ionics*, vol. 320, pp. 378-386, 2018.

[33] M. You, X. Huang, M. Lin, Q. Tong, X. Li, Y. Ruan, and Y. Yang, "Preparation of $LiCoMnO_4$ assisted by hydrothermal approach and its electrochemical performance," *American Journal of Engineering and Applied Sciences*, vol. 9, no. 2, pp. 396-405, 2016.

[34] J.-E. Zhou, J. Chen, X. Zhang, A. Zeb, and X. Lin, "Molecular and atomic manipulation of metal-organic framework-derived $LiCoMnO_4$: An oxygen-deficient strategy for advanced lithium storage," *Journal of Energy Chemistry*, vol. 75, pp. 216-228, 2022.

[35] H.-F. Lin, Y.-R. Tsai, C.-H. Cheng, S.-T. Cheng, D.-Z. Chen, and N.-Y. Wu, "Structural and electrochemical properties of $LiCoMnO_4$ doped with Mg, La, and F as a high-voltage cathode material for lithium ion batteries," *Electrochimica Acta*, vol. 427, pp. 1-14, 2022.

[36] S. Liu, H. He, and C. Chang, "Understanding the improvement of fluorination in 5.3 V $LiCoMnO_4$ spinel," *Journal of Alloys and Compounds*, vol. 860, pp. 1-9, 2021.

[37] D. Pasero, S. de Souza, N. Reeves, and A. R. West, "Oxygen content and electrochemical activity of $LiCoMnO_4$–δ," *Journal of Materials Chemistry*, vol. 15, no. 41, pp. 4435-4440, 2005.

[38] J. Ko, and Y. S. Yoon, "Recent progress in LiF materials for safe lithium metal anode of rechargeable batteries: Is LiF the key to commercializing Li metal batteries?," *Ceramics International*, vol. 45, no. 1, pp. 30-49, 2019.

[39] A. Windmüller, C. A. Bridges, C.-L. Tsai, S. Lobe, C. Dellen, G. M. Veith, M. Finsterbusch, S. Uhlenbruck, and O. Guillon, "Impact of fluorination on phase stability, crystal chemistry, and capacity of $LiCoMnO_4$ high voltage spinels," *ACS Applied Energy Materials*, vol. 1, no. 2, pp. 715-724, 2018.

[40] J. Mosa, and M. Aparicio, "lithium intercalation materials for battery prepared by sol–gel method," in *Handbook of Sol-Gel*

Science and Technology, Springer International Publishing, pp. 1-36, 2017.

[41] A. E. Danks, S. R. Hall, and Z. Schnepp, "The evolution of 'sol–gel' chemistry as a technique for materials synthesis," *Materials Horizons*, vol. 3, no. 2, pp. 91-112, 2016.

[42] N. Amdouni, F. Gendron, A. Mauger, H. Zarrouk, and C. M. Julien, "$LiMn_2{-}yCo_yO_4$ ($0 \leq y \leq 1$) intercalation compounds synthesized from wet-chemical route," *Materials Science and Engineering: B*, vol. 129, no. 1-3, pp. 64-75, 2006.

[43] A. S. Rahim, N. Aziz, N. A. M. Nor, and Z. Osman, "$LiNi_{0.5}Mn_{1.5}O_4$ cathode material prepared by sol–gel method," *Molecular Crystals and Liquid Crystals*, vol. 695, no. 1, pp. 10-18, 2020.

[44] J. L. Wang, Z. H. Li, J. Yang, J. J. Tang, J. J. Yu, W. B. Nie, G. T. Lei, and Q. Z. Xiao, "Effect of Al-doping on the electrochemical properties of a three-dimensionally porous lithium manganese oxide for lithium-ion batteries," *Electrochimica Acta*, vol. 75, pp. 115-122, 2012.

[45] Y.-S. Lee, N. Kumada, and M. Yoshio, "Synthesis and characterization of lithium aluminum-doped spinel ($LiAl_xMn_{2-x}O_4$) for lithium secondary battery," *Journal of Power Sources*, vol. 96, no. 2, pp. 376-384, 2001.

[46] H. Shigemura, M. Tabuchi, H. Kobayashi, H. Sakaebe, A., Hirano, and Kageyama, H., "Structural and electrochemical properties of $Li(Fe,Co)_xMn_{2-x}O_4$ solid solution as 5 V positive electrode materials for Li secondary batteries," *Journal of Materials Chemistry*, vol. 12, no. 6, pp. 1882-1891, 2002.

[47] T. Li, K. Chang, A. M. Hashem, A. E. Abdel-Ghany, R. S. El-Tawil, H. Wang, H. El-Mounayri, A. Tovar, L. Zhu, and C. M. Julien, "Structural and electrochemical properties of the high Ni content spinel $LiNiMnO_4$," *Electrochem,* vol. 2, no. 1, pp. 95-117, 2021.

[48] Z.-M. Yu, and L.-C., Zhao, "Structure and electrochemical properties of $LiMn_2O_4$," *Transactions of Nonferrous Metals Society of China,* vol. 17, no. 3, pp. 659-664, 2007.

[49] G. Y. Liu, J. M. Guo, Y. N. Li, and B. S. Wang, "Effect of single or double calcination on $LiMn_2O_4$ prepared by a solution combustion synthesis," *Advanced Materials Research*, vol. 216, pp. 134-137, 2011.

[50] C. Peng, H. Bai, M. Xiang, C. Su, G. Liu, and J. Guo, "Effect of calcination temperature on the electrochemical properties of spinel $LiMn_2O_4$ prepared by solid-state combustion synthesis," *International Journal of Electrochemical Science*, vol. 9, no. 4, pp. 1791-1798, 2014.

[51] E. Bulut, A. Örnek, and M. Özacar, "Effect of calcination temperature on synthesis of $LiMn_2O_4$ cathode active nanoparticles for rechargeable Li-ion batteries," *Advanced Science, Engineering and Medicine*, vol. 3, no. 1, pp. 67-71, 2011.

[52] S. H. Ju, and D.-W. Kim, "Effect of calcination temperature on the structure and electrochemical performance of $LiMn_{1.5}Ni_{0.5}O_4$ cathode materials," *Bulletin of the Korean Chemical Society*, vol. 34, no. 1, pp. 59-62, 2013.

[53] B.-Y. Lee, C.-T. Chu, M. Krajewski, M. Michalska, and J.-Y. Lin, "Temperature-controlled synthesis of spinel lithium nickel manganese oxide cathode materials for lithium-ion batteries," *Ceramics International*, vol. 46, no. 13, pp. 20856-20864, 2020.

[54] J. Zheng, P. Yan, L. Estevez, C. Wang, and J.-G. Zhang, "Effect of calcination temperature on the electrochemical properties of nickel-rich $LiNi_{0.76}Mn_{0.14}Co_{0.10}O_2$ cathodes for lithium-ion batteries," *Nano Energy*, vol. 49, pp. 538-548, 2018.

[55] B. Cao, W. Chen, and H. Fang, "Facile synthesis of spinel $LiMn_2O_4$ cathode material from nanoscale Mn_3O_4 for lithium-ion batteries," *International Journal of Electrochemical Science*, vol. 20, no. 8, 2025.

[56] A. Balakrishnan, P. Pizette, C. L. Martin, S. V. Joshi, and B. P. Saha, "Effect of particle size in aggregated and agglomerated ceramic powders," *Acta Materialia*, vol. 58, no. 3, pp. 802-812, 2010.

[57] I. Taniguchi, N. Fukuda, and M. Konarova, "Synthesis of spherical $LiMn_2O_4$ microparticles by a combination of spray pyrolysis and drying method," *Powder Technology*, vol. 181, no. 3, pp. 228-236, 2008.

[58] J. Zhang, J. Qiao, K. Sun, and Z. Wang, "Balancing particle properties for practical lithium-ion batteries," *Particuology*, vol. 61, pp. 18-29, 2022.

[59] A. Hoffmann, E. A. Heider, C. Dreer, C. Pfeifer, and M. Wohlfahrt-Mehrens, "Influence of the mixing and dispersing process on the slurry properties and the microstructure and performance of ultrathick cathodes for lithium-ion batteries," *Energy Technology*, vol. 11, no. 5, 2022.

[60] K. Konda, S. B. Moodakare, P. L. Kumar, M. Battabyal, J. R. Seth, V. A. Juvekar, and R. Gopalan, "comprehensive effort on electrode slurry preparation for better electrochemical performance of $LiFePO_4$ battery," *Journal of Power Sources*, vol. 480, 2020.

[61] N. Anansuksawat, T. Sangsanit, S. Prempluem, K. Homlamai, W. Tejangkura, and M. Sawangphruk, "How uniform particle size of NMC90 boosts lithium ion mobility for faster charging and discharging in a cylindrical lithium ion battery cell," *Chemical Science*, vol. 15, no. 6, pp. 2026-2036, 2024.

[62] W. Choi, H.-C. Shin, J. M. Kim, J.-Y. Choi, and W.-S. Yoon, "Modeling and applications of electrochemical impedance spectroscopy (EIS) for lithium-ion batteries," *Journal of Electrochemical Science and Technology*, vol. 11, no. 1, pp. 1-13, 2020.

[63] W. Hu, Y. Peng, Y. Wei, and Y. Yang, "Application of electrochemical impedance spectroscopy to degradation and aging research of lithium-ion batteries," *The Journal of Physical Chemistry C*, vol. 127, no. 9, pp. 4465-4495, 2023.

[64] K. Ariyoshi, Z. Siroma, A. Mineshige, M. Takeno, T. Fukutsuka, T. Abe, and S. Uchida, "Electrochemical impedance spectroscopy part 1: Fundamentals," *Electrochemistry*, vol. 90, no. 10, pp. 102007-102007, 2022.

[65] O. Nyamaa, G. H. Kang, S. C. Huh, J. H. Yang, T. H. Nam, and J. P. Noh, "Unraveling the mechanism and practical implications of the sol-gel synthesis of spinel $LiMn_2O_4$ as a cathode material for Li-Ion batteries: Critical effects of cation distribution at the matrix level," *Molecules*, vol. 28, no. 8, 2023.

[66] C. Bischoff, O. Fitz, C. Schiller, H. Gentischer, D. Biro, and H.-M. Henning, "Investigating the impact of particle size on the performance and internal resistance of aqueous zinc ion batteries with a manganese sesquioxide cathode," *Batteries,*

vol. 4, no. 3, 2018.

[67] P. Cofré, A. Quispe, and M. Grágeda, "Effect of particle-size distribution on $LiFePO_4$ cathode electrochemical performance in Li-ion cells," *Revista Mexicana de Ingeniería Química*, vol. 21, no. 2, pp. 1-12, 2022.

[68] W. Liang, P. Wang, H. Ding, B. Wang, and S. Li, "Granularity control enables high stability and elevated-temperature properties of micron-sized single-crystal $LiNi_{0.5}Mn_{1.5}O_4$ cathodes at high voltage," *Journal of Materiomics*, vol. 7, no. 5, pp. 1049-1060, 2021.